

Reconciling perturbative approaches in phonon assisted transport junctions

Bijay Kumar Agarwalla and Dvira Segal¹

Chemical Physics Theory Group, Department of Chemistry, and Centre for Quantum Information and Quantum Control, University of Toronto, 80 Saint George St., Toronto, Ontario, Canada M5S 3H6

(Dated: 9 June 2021)

We present consistent results for molecular conduction using two central-complementary approaches: the non-equilibrium Green's function technique and the quantum master equation method. Our model describes electronic conduction in a donor-acceptor junction in which electron transfer is coupled to nuclear motion, modeled by a harmonic vibrational mode. This primary mode is further coupled to secondary phonon modes, a thermal bath. Assuming weak electron-phonon coupling but arbitrary large molecule-metal hybridization, we compute several non-equilibrium transport quantities: the mean phonon number of the primary mode, charge current statistics. We further present scaling relations for the cumulants valid in the large voltage regime. Our analysis illustrates that the non-equilibrium Green's function technique and the quantum master equation method can be worked out consistently, when taking into account corresponding scattering processes.

I. INTRODUCTION

Studies of charge transfer in single-molecule junctions¹⁻⁴ capture significant attention for various reasons: (i) Molecular junctions offer a unique playground for exploring basic quantum effects in dynamics e.g., interference between different transport pathways^{5,6}, and (ii) molecules can serve as building blocks for electronic devices such as molecular diodes^{7,8}, sensors, switches, thermo and opto-electronic devices⁹.

Electron-nuclei interactions are central to molecular electronic applications¹⁰. Nuclear motion in conducting molecules and the surroundings governs effects such as local heating of the junction, which may lead to instabilities¹¹, and incoherent tunnelling processes, responsible for the development of ohmic conduction¹². These effects can be captured within simple models: The celebrated Anderson-Holstein model includes a single electronic site embedded between metals, further coupled to a single vibration, or a harmonic bath¹³⁻²⁶. A different class of problems, relevant as well to photovoltaic devices²⁷, concerns donor-acceptor type molecular systems, with two electronic sites coupled to molecular vibrations^{11,28-34}. Experimentally, inelastic electron tunnelling spectroscopy can identify molecular vibrations participating in the transport process³⁵⁻³⁷.

Besides measurements of current-voltage characteristics^{1,3}, the distribution function of current fluctuations, or the *full counting statistics* (FCS), can be received experimentally by counting the number of tunneling electrons through a conductor within a given time period^{38,39}. FCS provides a complete picture of the transport problem in the steady state regime with cumulants of current conveying information over interactions such electron correlation effects, and the junction's geometry.

From a theoretical perspective, two eminent perturbative methods are routinely used to investigate transport properties in molecular junctions: the non-equilibrium Green's function (NEGF) technique⁴⁰⁻⁴⁴, and the quan-

tum master equation (QME) approach⁴⁵⁻⁵². Both schemes are perturbative in nature, yet are developed along separate lines, identifying different interaction Hamiltonians for the perturbative expansion.

The NEGF theory is exact for bilinear metal-molecule Hamiltonians, but it is perturbative in nonlinear interaction terms within the subsystem (molecule), e.g., electron-vibration coupling or electron-electron interactions. It hands over a formally exact expression for currents, the Meir-Wingreen (MW) formula⁵³, written in terms of the so-called nonlinear self-energy. The MW formula was recently generalized to accommodate higher order fluctuations^{54,55}. Furthermore, the NEGF approach can be used to reach analytical expressions for the cumulant generating function (CGF), which directly provides the mean current and its fluctuations³². QME approaches, in contrast, are typically developed in the energy basis of the subsystem, thus treating, in an exact manner, internal-molecular nonlinear interactions. However, QME methods are typically made perturbative in the molecule-metal coupling^{46,50}, thus restricted to handle only low-order processes in the tunnelling strength. Equivalence between NEGF and QME in molecular transport problems has been demonstrated only in the weak molecule-metal coupling limit in specific situations^{56,57}.

In this paper, we show that NEGF and QME methods can be exercised in a compatible manner, to provide nonequilibrium quantities, particularly, *high order cumulants* of the current at *strong* metal-molecule coupling. This is achieved by working out the methods consistently, namely, by including the same inelastic scattering processes.

Our model includes two electronic levels, denoted as 'donor' and 'acceptor', following the chemistry literature on electron transfer. Charge transfer between these sites takes place via electron interaction with a local vibrational mode (primary phonon mode), e.g., a torsional mode within a biphenyl molecule³⁰. The primary mode is further coupled to a secondary phonon bath, allowing it to dissipate its excess energy. For a schematic repre-

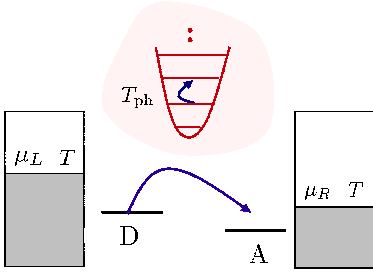


FIG. 1. Scheme of a biased donor-acceptor molecular junction with electron hopping between sites coupled to a (primary) harmonic vibrational mode, itself embedded in a (secondary) phononic environment.

resentation see Fig. 1. The donor-acceptor model was employed by Aviram and Ratner for proposing a molecular electronic diode⁵⁸. Recently, it was applied for exploring heating effects in molecular junctions^{11,28,29}, and quantum interference effects in molecular conduction³⁰ and thermoelectricity³¹.

In our treatment, we incorporate the molecule-metal hybridization exactly via a diagonalization procedure for the electronic part of the Hamiltonian, then perform a perturbation expansion for the electron-phonon interaction Hamiltonian. Following the QME approach, steady state observables are readily obtained, most importantly, with the fluctuation symmetry immediately satisfied⁵⁹. In contrast, in the NEGF scheme it is crucial to employ the so-called random phase approximation (RPA) so as to take into account corresponding scattering processes and satisfy the fluctuation theorem.

In Ref.^{32,33} we had investigated a similar setup—without the secondary bath. However, our focus in^{32,33} has been on comparing transport behavior in two situations: the case with a harmonic primary model, which was treated with NEGF, and a model with an anharmonic primary mode (a two-state impurity), handled by QME. Here, in contrast, we focus on reconciling NEGF and the QME techniques by applying them on *the same model*, as depicted in Fig. 1.

The paper is organized as follows. We introduce our model in Sec. II. In Sec. III, we show an agreement between the NEGF and QME methods by calculating the mean-phonon number. In Sec. IV, we obtain the CGF for charge and energy current statistics using NEGF, and explain how cumulants are to be obtained with the QME. We demonstrate with numerical simulations the equivalence between the two schemes for the first three current cumulants in Sec. V. We summarize our work in Sec. VI.

II. MODEL

We consider a minimal two-site molecule with the electronic states identified as donor (D) and acceptor (A). The molecule is placed between two metal leads including non-interacting electrons. Electron transfer between

the D and A sites takes place while exchanging energy with a molecular vibrational mode, designated as the “primary phonon”. This mode is coupled to a thermal environment including “secondary phonons”. We write down the total Hamiltonian as (we set $\hbar = k_B = e = 1$ throughout the paper),

$$\hat{H}_T = \hat{H}_{\text{el}} + \hat{H}_{\text{vib}} + \hat{H}_{\text{el-vib}}, \quad (1)$$

with

$$\begin{aligned} \hat{H}_{\text{el}} = & \epsilon_d \hat{c}_d^\dagger \hat{c}_d + \epsilon_a \hat{c}_a^\dagger \hat{c}_a + \sum_{l \in L} \epsilon_l \hat{c}_l^\dagger \hat{c}_l + \sum_{r \in R} \epsilon_r \hat{c}_r^\dagger \hat{c}_r \\ & + \sum_{l \in L} v_l (\hat{c}_l^\dagger \hat{c}_d + \hat{c}_d^\dagger \hat{c}_l) + \sum_{r \in R} v_r (\hat{c}_r^\dagger \hat{c}_a + \hat{c}_a^\dagger \hat{c}_r), \end{aligned} \quad (2)$$

where ϵ_d, ϵ_a are the donor and acceptor site energies, coupled to the left L and right R metal leads by real-valued hopping elements v_l and v_r , respectively. \hat{c}^\dagger and \hat{c} are fermionic creation and annihilation operators for the respective regions. \hat{H}_{vib} is the Hamiltonian for the vibrational degrees of freedom. It consists the primary phonon of frequency ω_0 , the secondary phonon bath, and a real-valued linear coupling term with matrix elements ν_j ,

$$\hat{H}_{\text{vib}} = \omega_0 \hat{b}_0^\dagger \hat{b}_0 + \sum_j \omega_j \hat{b}_j^\dagger \hat{b}_j + (\hat{b}_0^\dagger + \hat{b}_0) \sum_j \nu_j (\hat{b}_j^\dagger + \hat{b}_j). \quad (3)$$

The interaction between electrons in the junction and the primary mode is given by the “off-diagonal” model,

$$\hat{H}_{\text{el-vib}} = g [\hat{c}_d^\dagger \hat{c}_a + \hat{c}_a^\dagger \hat{c}_d] (\hat{b}_0^\dagger + \hat{b}_0). \quad (4)$$

Here \hat{b}_0 (\hat{b}_0^\dagger) and \hat{b}_j (\hat{b}_j^\dagger) are bosonic annihilation (creation) operators for vibrational modes with frequencies ω_0 and ω_j , respectively. The model has been justified in details in Ref.³². The quadratic electron Hamiltonian (2) can be diagonalized via a unitary transformation²⁸. The total Hamiltonian now reads

$$\begin{aligned} \hat{H}_T = & \hat{H}_{\text{vib}} + \sum_l \epsilon_l \hat{a}_l^\dagger \hat{a}_l + \sum_r \epsilon_r \hat{a}_r^\dagger \hat{a}_r \\ & + \sum_{l \in L, r \in R} g [\gamma_l \gamma_r^* \hat{a}_l^\dagger \hat{a}_r + h.c.] (\hat{b}_0^\dagger + \hat{b}_0), \end{aligned} \quad (5)$$

where the new fermionic operators $\hat{a}_{l,r}$ are related to the original operators according to

$$\begin{aligned} \hat{c}_d = & \sum_l \gamma_l \hat{a}_l, & \hat{c}_a = & \sum_r \gamma_r \hat{a}_r, \\ \hat{c}_l = & \sum_{l'} \eta_{ll'} \hat{a}_{l'}, & \hat{c}_r = & \sum_{r'} \eta_{rr'} \hat{a}_{r'}, \end{aligned} \quad (6)$$

with the dimensionless coefficients

$$\gamma_l = \frac{v_l}{\epsilon_l - \epsilon_d - \sum_{l'} \frac{v_{l'}^2}{\epsilon_l - \epsilon_{l'} + i\delta}}, \quad \eta_{ll'} = \delta_{ll'} - \frac{v_l \gamma_{l'}}{\epsilon_l - \epsilon_{l'} + i\delta}. \quad (7)$$

Here δ is a positive infinitesimal number introduced to ensure causality. Analogous expressions can be written

for the r set. The expectation values for the e.g. l number operators satisfy $\langle \hat{a}_l^\dagger \hat{a}_l \rangle = \delta_{ll'} f_L(\epsilon_l)$ with $f_L(\epsilon_l) = \{\exp[\beta_L(\epsilon_l - \mu_L)] + 1\}^{-1}$ the Fermi function of the left lead with the chemical potential μ_L and temperature $T_L = 1/\beta_L$.

The primary vibration suffers dissipation due to its coupling to the bosonic-phononic and fermionic-electronic environments. We now organize Eq. (5) in the following form, $\hat{H}_T = \hat{H}_0 + \hat{V}$. \hat{H}_0 comprises the non-interacting terms of the model (primary and secondary modes, electron baths), and \hat{V} includes the interaction Hamiltonian, between the primary mode and the different baths,

$$\hat{V} = (\hat{b}_0^\dagger + \hat{b}_0)(\hat{B}_{\text{el}} + \hat{B}_{\text{ph}}). \quad (8)$$

The baths' operators are,

$$\begin{aligned} \hat{B}_{\text{el}} &= g \left[\sum_{l,r} \gamma_l^* \gamma_r \hat{a}_l^\dagger \hat{a}_r + \gamma_l \gamma_r^* \hat{a}_r^\dagger \hat{a}_l \right], \\ \hat{B}_{\text{ph}} &= \sum_{\alpha} \nu_j (\hat{b}_j^\dagger + \hat{b}_j). \end{aligned} \quad (9)$$

The following expressions are central to our discussion below,

$$\begin{aligned} k_d^{\text{el/ph}} &= \int_{-\infty}^{\infty} d\tau e^{-i\omega_0\tau} \langle \hat{B}_{\text{el/ph}}(0) \hat{B}_{\text{el/ph}}(\tau) \rangle, \\ k_u^{\text{el/ph}} &= \int_{-\infty}^{\infty} d\tau e^{i\omega_0\tau} \langle \hat{B}_{\text{el/ph}}(0) \hat{B}_{\text{el/ph}}(\tau) \rangle, \end{aligned} \quad (10)$$

defining excitation (u) and relaxation (d) rate constants within the special-primary harmonic mode, between neighboring states, driven by either the electronic or the phononic reservoirs. In the above definition, the electronic rates are computed by taking an average with respect to the canonical state of the left and right metal leads, $\hat{\rho}_{\text{el}} = \hat{\rho}_L \hat{\rho}_R$, with $\hat{\rho}_\alpha = e^{-\beta_\alpha(\hat{H}_\alpha - \mu_\alpha \hat{N}_\alpha)} / Z_\alpha$; $\alpha = L, R$. Z_α is the partition function and $\hat{H}_{L,R}$ are the Hamiltonians for the left and right compartments, second and third terms in Eq. (5). The phonon-bath induced rates are evaluated with the average taken over the canonical distribution $\hat{\rho}_{\text{ph}} = e^{-\beta_{\text{ph}} \hat{H}_{\text{ph}}} / Z_{\text{ph}}$ with $\hat{H}_{\text{ph}} = \sum_j \omega_j \hat{b}_j^\dagger \hat{b}_j$, and the inverse temperature $\beta_{\text{ph}} = 1/T_{\text{ph}}$. The operators are written in the interaction representation, $\hat{B}(\tau) = e^{i\hat{H}_0\tau} \hat{B} e^{-i\hat{H}_0\tau}$. Using Eq. (9), it can be shown that

$$k_{u/d}^{\text{el}} = [k_{u/d}^{\text{el}}]^{L \rightarrow R} + [k_{u/d}^{\text{el}}]^{R \rightarrow L}, \quad (11)$$

where the directional rates are²⁸

$$\begin{aligned} [k_u^{\text{el}}]^{L \rightarrow R} &= \int_{-\infty}^{\infty} \frac{d\epsilon}{2\pi} f_L(\epsilon) (1 - f_R(\epsilon - \omega_0)) J_L(\epsilon) J_R(\epsilon - \omega_0), \\ [k_u^{\text{el}}]^{R \rightarrow L} &= \int_{-\infty}^{\infty} \frac{d\epsilon}{2\pi} f_R(\epsilon) (1 - f_L(\epsilon - \omega_0)) J_R(\epsilon) J_L(\epsilon - \omega_0), \\ [k_d^{\text{el}}]^{L \rightarrow R} &= \int_{-\infty}^{\infty} \frac{d\epsilon}{2\pi} f_L(\epsilon) (1 - f_R(\epsilon + \omega_0)) J_L(\epsilon) J_R(\epsilon + \omega_0), \\ [k_d^{\text{el}}]^{R \rightarrow L} &= \int_{-\infty}^{\infty} \frac{d\epsilon}{2\pi} f_R(\epsilon) (1 - f_L(\epsilon + \omega_0)) J_R(\epsilon) J_L(\epsilon + \omega_0). \end{aligned} \quad (12)$$

Here $J_\alpha(\omega)$ are spectral functions, of Lorentzian form, centered around the donor (ϵ_d) and acceptor (ϵ_a) site energies with the broadening $\Gamma_\alpha(\epsilon) = 2\pi \sum_{k \in \alpha} v_k^2 \delta(\epsilon_k - \epsilon)$,

$$\begin{aligned} J_L(\epsilon) &= g \frac{\Gamma_L(\epsilon)}{(\epsilon - \epsilon_d)^2 + \Gamma_L(\epsilon)^2/4}, \\ J_R(\epsilon) &= g \frac{\Gamma_R(\epsilon)}{(\epsilon - \epsilon_a)^2 + \Gamma_R(\epsilon)^2/4}. \end{aligned} \quad (13)$$

The electronic rates (12) are nonzero when (i) both leads are not fully occupied or empty, and (ii) the overlap between the spectral functions, differing by one quanta of energy, is non-negligible. The phonon-bath induced rates can be similarly evaluated,

$$k_u^{\text{ph}} = \Gamma_{\text{ph}}(\omega_0) n_{\text{ph}}(\omega_0), \quad k_d^{\text{ph}} = \Gamma_{\text{ph}}(\omega_0) [1 + n_{\text{ph}}(\omega_0)], \quad (14)$$

with the coupling energy

$$\Gamma_{\text{ph}}(\omega) = 2\pi \sum_j \nu_j^2 \delta(\omega - \omega_j), \quad (15)$$

and the Bose-Einstein occupation factor $n_{\text{ph}}(\omega) = [e^{\beta_{\text{ph}}\omega} - 1]^{-1}$. We also define the total rates which determine the dynamics of the primary mode,

$$k_d = k_d^{\text{el}} + k_d^{\text{ph}}, \quad k_u = k_u^{\text{el}} + k_u^{\text{ph}}. \quad (16)$$

Appendix A generalizes these definitions to include counting fields for charge and energy. In the next sections we calculate several observables far from equilibrium using the NEGF and QME methods, and demonstrate their agreement when the NEGF method is carefully performed to include all single-phonon electron scattering processes.

III. MEAN PHONON NUMBER

We compute here the mean phonon number for the primary mode,

$$\langle \hat{n} \rangle \equiv \langle \hat{b}_0^\dagger \hat{b}_0 \rangle. \quad (17)$$

We employ the NEGF technique under the RPA approximation, then the QME approach under the Born-Markov

and the secular approximations. Results are valid under the assumption of *weak* (second-order) electron-primary phonon interaction g , as well as weak primary-secondary phonon couplings ν_j .

A. NEGF approach

We define the contour-ordered phonon Green's function as

$$\begin{aligned} D(\tau, \tau') &\equiv -i \langle T_c \hat{X}(\tau) \hat{X}(\tau') \rangle, \\ &= -i \langle T_c \hat{X}_I(\tau) \hat{X}_I(\tau') e^{-i/\hbar \int d\tau_1 \hat{H}_{\text{el-vib}}^I(\tau_1)} \rangle \end{aligned} \quad (18)$$

where $\hat{X} = (\hat{b}_0 + \hat{b}_0^\dagger)$ is proportional to the primary phonon displacement operator. T_c is the contour-ordered operator responsible for rearrangement of the operators according to their contour time. In the second line, the operators are written in the interaction picture with respect to the noninteracting parts $\hat{H}_{\text{el}} + \hat{H}_{\text{vib}}$, the quadratic parts of the total Hamiltonian. The perturbative expansion generates terms of different orders in the electron-phonon coupling g , (but it is exact to all orders so far in the coupling of the primary phonon to the phonon bath). A naive perturbative calculation with diagrams up to a particular order of g leads to the *violation* of different symmetries preserving physical processes, such as the conservation of charge and energy currents. In order to restore basic symmetries, one has to sum over an infinite-subclass of diagrams, taking into account all electron scattering processes which are facilitated by the absorption or emission of a single quanta ω_0 . This can be done by employing the so-called random phase approximation (RPA)^{60,61} where a particular type of ring diagrams are summed over, see Fig. (2). We can represent this infinite summation in a closed Dyson-like (kinetic) equation for $D(\tau, \tau')$,

$$\begin{aligned} D(\tau, \tau') &= D_0(\tau, \tau') \\ &+ \int d\tau_1 \int d\tau_2 D_0(\tau, \tau_1) F(\tau_1, \tau_2) D(\tau_2, \tau') \end{aligned} \quad (19)$$

D_0 is the primary phonon's Green's function, and it includes the effect of the secondary phonon bath. F , the electron-hole propagator, involves both left and right lead

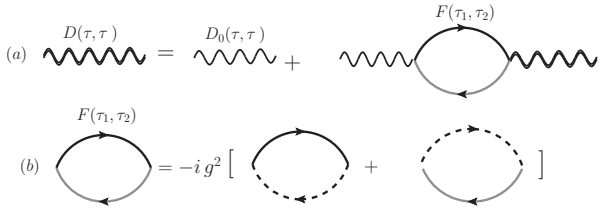


FIG. 2. (a) Dyson equation for the phonon Green's function $D(\tau, \tau')$ in contour time. (b) Electron-hole propagator $F(\tau, \tau')$. The solid and dashed lines represent the unperturbed Green's functions g_l and g_r for the leads, respectively.

electron Green's function (unperturbed), and it describes electron hopping processes from L to R and vice versa, assisted by scatterings with phonon modes. It is given as

$$\begin{aligned} F(\tau_1, \tau_2) &= -ig^2 \sum_{l \in L, r \in R} |\gamma_l|^2 \gamma_r^2 [g_l(\tau_1, \tau_2) g_r(\tau_2, \tau_1) \\ &+ g_r(\tau_1, \tau_2) g_l(\tau_2, \tau_1)]. \end{aligned} \quad (20)$$

This function is symmetric under the exchange of the contour time parameters τ_1 and τ_2 . The free (unperturbed) electronic Green's functions are

$$\begin{aligned} g_l(\tau_1, \tau_2) &= -i \langle T_c \hat{a}_l(\tau_1) \hat{a}_l^\dagger(\tau_2) \rangle_L, \\ g_r(\tau_1, \tau_2) &= -i \langle T_c \hat{a}_r(\tau_1) \hat{a}_r^\dagger(\tau_2) \rangle_R, \end{aligned} \quad (21)$$

with the average performed over the respective grand canonical distribution functions with well-defined temperatures T_α and chemical potentials μ_α , $\alpha = L, R$. In the long-time (steady state) limit, different real-time components of D can be obtained. The convolution in time domain results in a multiplicative form in frequency domain,

$$\begin{aligned} \mathbf{D}(\omega) &= \begin{bmatrix} D^t(\omega) & D^<(\omega) \\ D^>(\omega) & D^{\bar{t}}(\omega) \end{bmatrix} = [\mathbf{D}_0^{-1}(\omega) - \mathbf{F}(\omega)]^{-1} = \\ &= \begin{bmatrix} [D_0^<]^{-1}(\omega) - \Sigma_{\text{ph}}^<(\omega) - F^t(\omega) & \Sigma_{\text{ph}}^<(\omega) + F^<(\omega) \\ \Sigma_{\text{ph}}^>(\omega) + F^>(\omega) & -[D_0^>]^{-1}(\omega) - \Sigma_{\text{ph}}^>(\omega) - F^{\bar{t}}(\omega) \end{bmatrix}^{-1}, \end{aligned} \quad (22)$$

where $t, \bar{t}, <, >$ are the time ordered, anti-time ordered, lesser and greater components of the Green's function. The primary phonon retarded Green's function is

$$[D_0^r(\omega)]^{-1} = (\omega^2 - \omega_0^2)/2\omega_0 - \Sigma_{\text{ph}}^r \quad (23)$$

with Σ_{ph} the self energy due to the coupling of the mode to the phonon bath. For the mean phonon number, we are interested in the lesser $D^<(\omega)$ and greater $D^>(\omega)$ components. This can be readily calculated by inverting the 2×2 matrix which results in

$$D^{</>}(\omega) = \frac{\Pi^{</>}(\omega)}{\left[\frac{\omega^2 - \omega_0^2}{2\omega_0} - \left(\frac{\Pi^t - \Pi^{\bar{t}}}{2} \right)^2 + A_0(\omega) \right]}, \quad (24)$$

with the total self-energy due to both electronic and phononic baths,

$$\begin{aligned} \Pi^{</>}(\omega) &= \Sigma_{\text{ph}}^{</>}(\omega) + F^{</>}(\omega), \\ \Pi^{t/\bar{t}}(\omega) &= \Sigma_{\text{ph}}^{t/\bar{t}}(\omega) + F^{t/\bar{t}}(\omega). \end{aligned} \quad (25)$$

The function $A_0(\omega)$ is written solely in terms of $\Pi^{</>}(\omega)$ as

$$A_0(\omega) = -\frac{1}{4} [\Pi^>(\omega) - \Pi^<(\omega)]^2, \quad (26)$$

and it will emerge as the central quantity in this problem. The mean-square displacement, in steady-state, can be

readily obtained from the phonon Green's function as

$$\begin{aligned} \langle \hat{X}^2 \rangle &= \frac{i}{2} \int_{-\infty}^{\infty} \frac{d\omega}{2\pi} [D^<(\omega) + D^>(\omega)], \\ &= \frac{i}{2} \int_{-\infty}^{\infty} \frac{d\omega}{2\pi} \frac{\Pi^<(\omega) + \Pi^>(\omega)}{\left[\frac{\omega^2 - \omega_0^2}{2\omega_0} - \left(\frac{\Pi^+ - \Pi^-}{2} \right)^2 \right]^2 + A_0(\omega)}. \end{aligned} \quad (27)$$

The integration can be performed to include terms to the lowest nontrivial order in the electron-phonon coupling (order g^2) and in Γ_{ph} . We employ the residue theorem to perform the integration. The poles are located at (correct up-to the second order) $\pm\{\omega_0 + \text{Re}[\Pi^R(\omega_0)] \pm i\sqrt{A_0(\omega_0)}\}$. The integration in (27) then results in

$$\int_{-\infty}^{\infty} \frac{d\omega}{2\pi} D^{</>}(\omega) = \frac{\Pi^{</>}(\omega_0)}{\sqrt{A_0(\omega_0)}}. \quad (28)$$

Using the expressions for the free (unperturbed) left and right lead Green's functions in Eq. (21), we identify the elements $F^{</>}, \Sigma_{ph}^{</>}$ in terms of mode excitation and relaxation rates as induced by the electronic and phononic baths, (12) and (14), respectively. Explicitly, at the vibrational frequency ω_0 , we get³²

$$F^>(\omega_0) = -ik_d^{\text{el}}, \quad F^<(\omega_0) = -ik_u^{\text{el}}. \quad (29)$$

and

$$\Sigma_{ph}^>(\omega_0) = -ik_d^{\text{ph}}, \quad \Sigma_{ph}^<(\omega_0) = -ik_u^{\text{ph}}, \quad (30)$$

From Eq. (26) we obtain $\sqrt{A_0(\omega_0)} = \frac{1}{2}(k_d - k_u)$ assuming $k_d > k_u$, with the total rates defined in Eq. (16). The final result is thus

$$\langle \hat{X}^2 \rangle = \frac{k_d + k_u}{k_d - k_u}, \quad (31)$$

and the mean phonon number is given by

$$\langle \hat{n} \rangle = \frac{1}{2} [\langle \hat{X}^2 \rangle - 1] = \frac{k_u}{k_d - k_u}. \quad (32)$$

B. QME approach

We compute here the mean phonon number for the primary mode following a QME- projection operator technique. First, we identify the baths—to be traced over. Singling out the primary phonon as the system of interest, our model system (Fig. 1) includes two environments: the electronic degrees of freedom prepare a nonequilibrium electronic bath, and the secondary phonons constitute a second thermal bath.

In standard QME approaches, the perturbation expansion is done with respect to the metal-molecule coupling⁴⁶. Here, instead, we treat the interaction of the primary mode with the electron and phonon baths as weak-perturbative, but the hybridization of the D and A electronic states to the metals is treated exactly, with the

help of the diagonalization procedure. In second order of perturbation theory with respect to g and ν_j , and after a Markov approximation, the reduced density matrix equation for the primary harmonic mode of frequency ω_0 takes the following form⁶²

$$\begin{aligned} \dot{\rho}_s(t) &= -i[\hat{V}(t), \rho_s(0)] \\ &- \int_0^\infty d\tau \text{Tr}_{\text{el,ph}} \{ [\hat{V}(t), [\hat{V}(\tau), \rho_s(t) \otimes \hat{\rho}_L \hat{\rho}_R \otimes \hat{\rho}_{\text{ph}}]] \}, \end{aligned} \quad (33)$$

with the operators written in the interaction representation with respect to \hat{H}_0 . The trace is performed over the electronic and the secondary-phonon bath degrees of freedom, with initial conditions given by equilibrium density matrices, as explained below Eq. (10).

Further imposing the secular approximation, i.e., decoupling the evolution of diagonal and off-diagonal elements, we obtain a kinetic-type equation for the populations of the primary mode, $p_n \equiv \langle n | \rho_s(t) | n \rangle$,

$$\dot{p}_n = -[n k_d + (n+1) k_u] p_n + (n+1) k_d p_{n+1} + n k_u p_{n-1}, \quad (34)$$

with the rates (16). The steady state solution, $\dot{p}_n = 0$, is obtained by using a trial form $p_n = c y^n$, which results in the normalized solution⁴⁸

$$p_n = \left(1 - \frac{k_u}{k_d}\right) \left(\frac{k_u}{k_d}\right)^n. \quad (35)$$

The average phonon number can now be directly evaluated,

$$\langle \hat{n} \rangle = \sum_n n p_n = \frac{k_u}{k_d - k_u}. \quad (36)$$

This result precisely matches the NEGF expression (32). The QME derivation reveals that this result does not rely on quantum coherence effects within the primary mode, which may contribute only in higher orders of the electron-phonon coupling energy.

IV. CHARGE CURRENT STATISTICS

We study the statistics (distribution) of charge and energy currents from the so-called characteristic function, which is related to the distribution function via a Fourier transform. Following the two-time measurement procedure⁶³, we define the characteristic function as^{59,64,65},

$$\mathcal{Z}(\lambda_e, \lambda_p) = \left\langle e^{i\lambda_e \hat{H}_R + i\lambda_p \hat{N}_R} e^{-i\lambda_e \hat{H}_R^H(t) - i\lambda_p \hat{N}_R^H(t)} \right\rangle. \quad (37)$$

Here, λ_e and λ_p are counting fields for energy and particles, respectively. $\langle \dots \rangle$ represents an average with respect to the total density matrix at the initial time, $\hat{\rho}_T(0) = \hat{\rho}_L(0) \hat{\rho}_R(0) \otimes \hat{\rho}_{\text{ph}}(0) \otimes \rho_s(0)$, a factorized-product form for the three baths (two metals, secondary phonons)

and the primary mode (system, denoted by s). The baths are prepared in thermal equilibrium, as explained below Eq. (10). The operators are written here in the Heisenberg representation and $\hat{H}_R = \sum_r \epsilon_r \hat{a}_r^\dagger \hat{a}_r$, $\hat{N}_R = \sum_r \hat{a}_r^\dagger \hat{a}_r$. The CGF is defined as follows,

$$\mathcal{G}(\lambda_e, \lambda_p) = \lim_{t \rightarrow \infty} \frac{1}{t} \ln \mathcal{Z}(\lambda_e, \lambda_p). \quad (38)$$

The steady state current and higher order cumulants can be readily obtained by taking derivatives with respect to the counting fields. Specifically, the cumulants of the particle current are given as

$$\begin{aligned} C_m &\equiv \langle I_p^m \rangle \\ &\equiv \left. \frac{\partial^m \mathcal{G}(\lambda_e, \lambda_p)}{\partial (i\lambda_p)^m} \right|_{\lambda=0}, \quad m = 1, 2, \dots \end{aligned} \quad (39)$$

where $\lambda = (\lambda_e, \lambda_p)$. In Sec. IV A we provide an analytic expression for the CGF (38) from an NEGF formalism. This allows us to reach closed-form expressions for the current cumulants, given in terms of counting-field dependent rates. Using the QME, in Sec. IV B we directly-numerically compute cumulants, by using a recursive algorithm. Numerical results as presented in Sec. V confirm that the two methods yield equivalent results for the first three cumulants.

A. NEGF approach

We had recently derived an analytic expression for the CGF for the model of Fig. 1—without a secondary phonon bath—using an NEGF approach, by following an RPA scheme³² We now describe how to generalize this study to include this additional dissipation channel. It can be shown that⁴⁰

$$\ln \mathcal{Z}_{\text{RPA}}(\lambda_e, \lambda_p) = -\frac{1}{2} \text{Tr}_\tau \ln [I - D_0(\tau, \tau') \tilde{F}(\tau, \tau')], \quad (40)$$

where tilde refers to $\lambda = (\lambda_e, \lambda_p)$ -dependent quantities. D_0 follows the same definition as before, but the electron-hole propagator is now modified due to the counting fields³²,

$$\begin{aligned} \tilde{F}(\tau_1, \tau_2) &= -ig^2 \sum_{l \in L, r \in R} |\gamma_l|^2 \gamma_r^2 [g_l(\tau_1, \tau_2) \tilde{g}_r(\tau_2, \tau_1) \\ &\quad + \tilde{g}_r(\tau_1, \tau_2) g_l(\tau_2, \tau_1)]. \end{aligned} \quad (41)$$

The greater and lesser components of \tilde{F} can be expressed by the counting-fields dependent rates,

$$\tilde{F}^{>/<}(\omega_0) = -i\tilde{k}_{d/u}^{\text{el}}, \quad (42)$$

see definition in the Appendix. Repeating the procedure of Ref.³²—with an additional-secondary phonon bath—we receive the CGF

$$\mathcal{G}(\lambda) = \frac{1}{2}(k_d - k_u) - \frac{1}{2} \sqrt{(k_u + k_d)^2 - 4\tilde{k}_d \tilde{k}_u}. \quad (43)$$

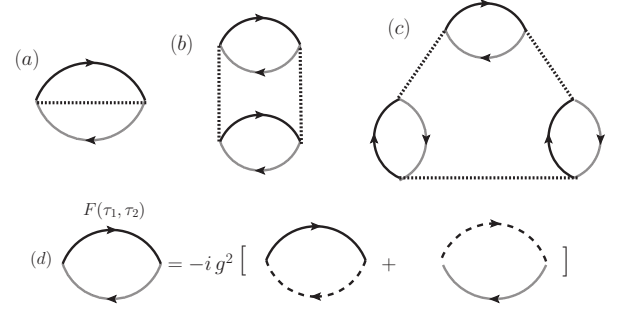


FIG. 3. Ring-type Feynman diagrams in contour time. (a) Second-order, (b) fourth-order, and (c) sixth-order diagrams in the electron-phonon coupling. The dotted line represents the phonon Green's function D_0 . (d) The closed loops are the electron-hole propagator \tilde{F} with solid and dotted lines corresponding to bare left and right-lead Green's functions.

This expression is correct up to second-order in the primary phonon-electron and primary phonon-secondary phonon couplings. The charge current immediately follows,

$$\langle I_p \rangle \equiv \left. \frac{\partial \mathcal{G}(\lambda)}{\partial (i\lambda_p)} \right|_{\lambda=0} = \frac{(k_u^{\text{el}})' k_d + (k_d^{\text{el}})' k_u}{k_d - k_u}, \quad (44)$$

with $(k_{u/d}^{\text{el}})'$ the difference between electronic rates, see Eq. (A4). The particle current can also be expressed in terms of mean phonon number, or the mean-square displacement, as

$$\begin{aligned} \langle I_p \rangle &= (k_u^{\text{el}})'(1 + \langle \hat{n} \rangle) + (k_d^{\text{el}})' \langle \hat{n} \rangle, \\ &= \langle \hat{X}^2 \rangle \left[(k_u^{\text{el}})' + (k_d^{\text{el}})' \right] + \frac{1}{2} \left[(k_u^{\text{el}})' - (k_d^{\text{el}})' \right]. \end{aligned} \quad (45)$$

The fluctuation (noise) in the charge current can be similarly organized,

$$\begin{aligned} \langle S_p \rangle &\equiv \left. \frac{\partial^2 \mathcal{G}(\lambda)}{\partial (i\lambda_p)^2} \right|_{\lambda=0} = \frac{k_u^{\text{el}} k_d + k_d^{\text{el}} k_u + 2(k_u^{\text{el}})'(k_d^{\text{el}})'}{k_d - k_u} \\ &\quad + \frac{2}{(k_d - k_u)} \langle I_p \rangle^2. \end{aligned} \quad (46)$$

The first term in $\langle S_p \rangle$ is referred to as the equilibrium noise (although it depends on the non-equilibrium condition), the second term adds a purely non-equilibrium contribution.

In the absence of the secondary phonon bath, the above expressions can be simplified to give

$$\langle I_p \rangle = 2 \frac{k_d^{R \rightarrow L} k_u^{R \rightarrow L} - k_d^{L \rightarrow R} k_u^{L \rightarrow R}}{k_d^{\text{el}} - k_u^{\text{el}}}. \quad (47)$$

The Fano factor $F \equiv \langle S_p \rangle / \langle I_p \rangle$ now obeys

$$\begin{aligned} F &= \frac{2\langle I_p \rangle}{k_d^{\text{el}} - k_u^{\text{el}}} \\ &\quad + 2 \frac{k_d^{R \rightarrow L} k_u^{R \rightarrow L} + k_d^{L \rightarrow R} k_u^{L \rightarrow R}}{k_d^{R \rightarrow L} k_u^{R \rightarrow L} - k_d^{L \rightarrow R} k_u^{L \rightarrow R}}. \end{aligned} \quad (48)$$

Note that in the absence of the secondary bath the system may develop the so called ‘‘vibrational instability’’ effect, an uncontrolled heating of the junction^{11,28}. At large bias, we reach $k_d^{\text{el}} \sim k_u^{\text{el}}$ (and even $k_d^{\text{el}} < k_u^{\text{el}}$), resulting in the blow-up of current. This physical instability can be relaxed once excess heat within the primary mode is allowed to dissipate into secondary phonon modes. In this case, the denominator in Eq. (44) is given by $k_d - k_u = k_d^{\text{el}} - k_u^{\text{el}} + \Gamma_{\text{ph}}$, which is positive even at high bias, as long as Γ_{ph} is large enough.

B. QME approach

The NEGF formalism furnishes a closed-form expression for the CGF. In the language of kinetic rate equations, this could be achieved by following an approach detailed in Ref.⁷⁰. Here, in contrast, we calculate high order cumulants directly from the Liouvillian. This approach is specifically useful as it is not limited to har-

monic systems, and could be implemented to describe junctions with anharmonic modes.

In the QME approach, the FCS can be obtained by following a counting field dependent master equation for ρ_λ^s , the reduced density matrix of the primary mode. It is defined from Eq. (37),

$$\mathcal{Z}(\lambda_e, \lambda_p) = \text{Tr}_T[\rho_{\lambda_e, \lambda_p}^s(t)] = \text{Tr}_s[\rho_{\lambda_e, \lambda_p}^s(t)]. \quad (49)$$

To include charge and energy measurements, the electron-phonon coupling term in the Hamiltonian (5) is dressed by counting fields,

$$\hat{V}_{\pm\lambda/2} = (\hat{b}_0^\dagger + \hat{b}_0)(\hat{B}_{\pm\lambda/2}^{\text{el}} + \hat{B}_{\text{ph}}), \quad (50)$$

with

$$\hat{B}_{\pm\lambda/2}^{\text{el}} = g \left[\sum_{l,r} \gamma_l^* \gamma_r \hat{a}_l^\dagger \hat{a}_r e^{\mp \frac{i}{2}(\lambda_p + \epsilon_r \lambda_e)} + h.c. \right]. \quad (51)$$

The counting-field dependent density matrix equation for the primary mode can be written formally as³²

$$\begin{aligned} \dot{\rho}_\lambda^s(t) = & - \int_0^t dt' \text{Tr}_{\text{el,ph}} \left[\hat{V}_{-\lambda/2}(t) \hat{V}_{-\lambda/2}(t') \hat{\rho}_\lambda^T(t') + \hat{\rho}_\lambda^T(t') \hat{V}_{\lambda/2}(t') \hat{V}_{\lambda/2}(t) \right. \\ & \left. - \hat{V}_{-\lambda/2}(t') \hat{\rho}_\lambda^T(t') \hat{V}_{\lambda/2}(t) - \hat{V}_{-\lambda/2}(t) \hat{\rho}_\lambda^T(t') \hat{V}_{\lambda/2}(t') \right]. \end{aligned} \quad (52)$$

Recall that λ is a shorthand notation for both λ_e and λ_p . As demonstrated in Refs.^{28,32}, under the Born-Markov approximation and the secular approximation, we can write down the population dynamics for the vibrational state as

$$\dot{p}_n^\lambda(t) = -[nk_d + (n+1)k_u] p_n^\lambda + (n+1) \tilde{k}_d p_{n+1}^\lambda + n \tilde{k}_u p_{n-1}^\lambda, \quad (53)$$

with $p_n^\lambda(t) \equiv \langle n | \rho_\lambda^s(t) | n \rangle$, $n = 0, 1, 2, \dots$. It is convenient to condense these equations into a matrix form,

$$|\dot{p}^\lambda\rangle = \tilde{\mathcal{L}} |p^\lambda\rangle, \quad (54)$$

with $\tilde{\mathcal{L}}$ the λ -dependent Liouvillian. The long-time (steady state) limit provides the CGF,

$$\mathcal{G}(\lambda) = \lim_{t \rightarrow \infty} \frac{1}{t} \ln \mathcal{Z}(\lambda) = \lim_{t \rightarrow \infty} \frac{1}{t} \ln \langle I | p^\lambda(t) \rangle, \quad (55)$$

where $\langle I | = (1, 1, 1, \dots)^T$ is the identity vector. It is obvious from the above equation that the steady state CGF is given by the smallest eigenvalue of the dressed Liouvillian $\tilde{\mathcal{L}}$. However, because of its infinite dimensionality a closed-form expression for the eigenvalue is not feasible to obtain⁷⁰. The cumulants can however be calculated numerically following the Rayleigh-Schrödinger perturbation scheme as described in^{66,67}.

An analytical expression for the current can be recovered from Eq. (55) using the steady state solution of the

vibrational mode, Eq. (35),

$$\begin{aligned} \langle I_p \rangle &= \frac{\partial \mathcal{G}(\lambda)}{\partial (i\lambda_p)} \Big|_{\lambda=0} = \langle I | \mathcal{L}'(0) | p_{ss} \rangle, \\ &= (k_d^{\text{el}})' (p_1 + 2p_2 + 3p_3 + \dots) \\ &+ (k_u^{\text{el}})' (p_0 + 2p_1 + 3p_2 + \dots), \\ &= \frac{(k_d^{\text{el}})' k_u + (k_u^{\text{el}})' k_d}{k_d - k_u}, \end{aligned} \quad (56)$$

where

$$\mathcal{L}'(0) \equiv \frac{\partial \tilde{\mathcal{L}}}{\partial (i\lambda_p)} \Big|_{\lambda=0} = \begin{bmatrix} 0 & (k_d^{\text{el}})' & 0 & 0 & \dots & \dots & \dots \\ (k_u^{\text{el}})' & 0 & 2(k_d^{\text{el}})' & 0 & 0 & \dots & \dots \\ 0 & 2(k_u^{\text{el}})' & 0 & 3(k_d^{\text{el}})' & 0 & \dots & \dots \\ 0 & 0 & 3(k_u^{\text{el}})' & 0 & 4(k_d^{\text{el}})' & 0 & \dots \\ 0 & 0 & 0 & \dots & \dots & \dots & \dots \\ \dots & \dots & \dots & \dots & \dots & \dots & \dots \end{bmatrix} \quad (57)$$

and $|p_{ss}\rangle = |p_0, p_1, p_2, \dots\rangle$ is the column vector with the steady state populations. The expression for current, Eq. (56), matches with the NEGF result, Eq. (44).

To calculate higher order statistics, the main inputs are (i) higher order derivatives of the Liouvillian with respect to counting fields, (ii) the steady state solution of the vibrational states, and, (iii) the pseudoinverse matrix, which is explained below. For example, the second

cumulant, or the noise due to charge-fluctuation, is given by^{66,67}

$$\begin{aligned} \langle S_p \rangle &\equiv \frac{\partial^2 \mathcal{G}(\lambda)}{\partial (i\lambda_p)^2} \Big|_{\lambda=0} \\ &= \langle I | \mathcal{L}'(0) | p_{ss} \rangle - 2 \langle I | \mathcal{L}'(0) \mathcal{R} \mathcal{L}'(0) | p_{ss} \rangle. \end{aligned} \quad (58)$$

Here \mathcal{R} is the pseudoinverse, defined as $\mathcal{R} = \mathcal{Q} \mathcal{L}^{-1} \mathcal{Q}$ with $\mathcal{Q} = \mathcal{Q}^2 = 1 - \mathcal{P}$, $\mathcal{P} = \mathcal{P}^2 = |p_{ss}\rangle \langle I|$. Note that the pseudoinverse is a well-defined quantity; the inverse is performed in the subspace corresponding to \mathcal{Q} which excludes the zero eigenvalue of the Liouvillian. We calculate \mathcal{R} numerically by computing the eigenvalues and the corresponding left and right eigenvectors of \mathcal{L} ,

$$\mathcal{R} = \mathcal{Q} \mathcal{L}^{-1} \mathcal{Q} = \sum_{n \neq 0} \frac{1}{\gamma_n} \mathcal{Q} | R_n \rangle \langle \langle L_n | \mathcal{Q}, \quad (59)$$

where $\mathcal{L} | R_n \rangle = \gamma_n | R_n \rangle$, $\langle L_n | \mathcal{L} = \gamma_n \langle L_n |$. We have also used the fact that $\mathcal{Q} | p_{ss} \rangle = 0$. Note that the sum excludes the zero eigenvalue. Similarly, the third cumulant (skewness) can be obtained as⁶⁷

$$\begin{aligned} \langle I_p^3 \rangle &= \langle I | \mathcal{L}'''(0) + 6 \mathcal{L}'(0) \mathcal{R} \mathcal{L}'(0) \mathcal{R} \mathcal{L}'(0) - 3 \mathcal{L}''(0) \mathcal{R} \mathcal{L}'(0) \\ &\quad - 3 \mathcal{L}'(0) \mathcal{R} \mathcal{L}''(0) - 6 \mathcal{L}'(0) \mathcal{R}^2 \mathcal{L}'(0) | p_{ss} \rangle. \end{aligned} \quad (60)$$

V. RESULTS

A. Simulations

In this section, we present numerical results for the mode occupation, current, and cumulants far from equilibrium. In presenting these results, we have two objectives in mind: (i) Demonstrate that results for the cumulants, reached from NEGF and QME, perfectly agree. (ii) Examine the functionality of the junction under bias and find out what information does the current and its cumulants convey on the junction's microscopic parameters.

Simulations are performed in the wide-band limit for the the leads. For simplicity, we assume symmetric coupling, $\Gamma_{L,R}(\epsilon) = \Gamma$. We set the equilibrium Fermi level at zero and move the bias symmetrically about the Fermi energy with $\Delta\mu \equiv \mu_R - \mu_L$. We work with the following representative parameters: $\epsilon_d = \epsilon_a = \epsilon_0 = 0.2$ eV as the energies of the molecular electronic states, $\Gamma = 0.01 - 0.1$ eV for the metal-molecule hybridization, $g = 0.01$ eV as the electron-primary phonon coupling. The electronic temperature is set at $T_L = T_R = 100$ K, while the phonon bath is set at $T_{ph} = 300$ K. Our conclusions do not depend on this precise choice of parameters.

In Fig. 4a we study the average phonon number in the primary mode as a function of the bias difference using $\Gamma < \omega_0$. The average phonon number increases once the bias $\Delta\mu$ exceeds the value $2\epsilon_0 = 0.4$ eV, revealed by the peak structure in Fig. 4b. The second peak arises

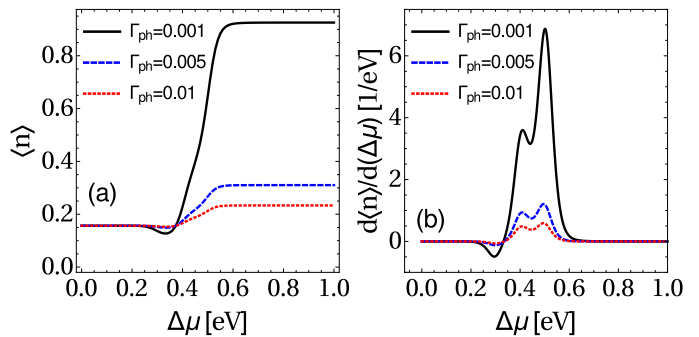


FIG. 4. (Color online) Heating and cooling of the primary mode. (a) Mean phonon number as a function of bias, and (b) its derivative, using different phonon damping rates. Parameters are $\epsilon_d = \epsilon_a = 0.2$ eV, $\omega_0 = 0.05$ eV, $g = 0.01$ eV, $\Gamma = 0.01$ eV, $T_L = T_R = 100$ K, $T_{ph} = 300$ K.

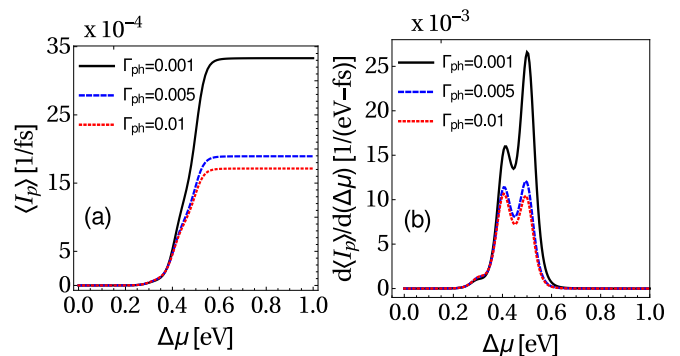


FIG. 5. (Color online) I-V characteristics of the junction. (a) Current and (b) differential conductance. Parameters are the same as in Fig. 4.

when the bias exceeds the value $2(\epsilon_0 + \omega_0)$. With increasing bias, the bath-induced excitation rate (k_u) increases, resulting in higher values for the average phonon number. The energy gap between the two peaks matches the value $2\omega_0$. Notice that the magnitude of the second peak at $\Delta\mu = 2(\epsilon_0 + \omega_0)$ is larger than the first one, because of the availability of many additional transport channels. With increasing Γ_{ph} , the mode dissipates its excess energy to the phonon bath, resulting in low values for the average phonon number. Interestingly, when the phonon damping rate is small, $\Gamma_{ph} = 0.001$ eV, a cooling effect takes place around $\Delta\mu = 0.3$ eV.

In Fig. 5 we plot the average current and the differential conductance, and observe similar trends as in the average phonon number. This can be understood from Eq. (45), where the current is expressed in terms of the mean phonon number. The current increases in two steps, and it saturates at high values of the bias.

Figures 6 and 7 illustrate the Fano factor $F = \langle S_p \rangle / \langle I_p \rangle$ and the normalized skewness $\langle I_p^3 \rangle / \langle I_p \rangle$, respec-

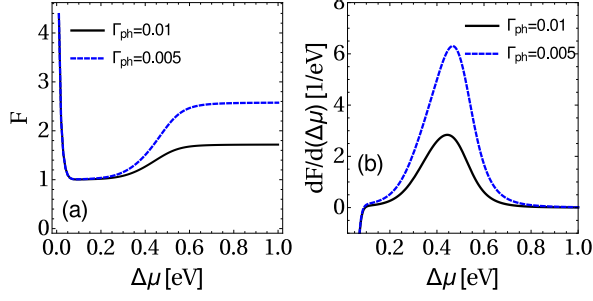


FIG. 6. (Color online) Second cumulant for charge transfer as obtained from the QME and NEGF methods (overlapping). The Fano factor is displayed as a function of bias voltage for $\Gamma = 0.1$ eV, other parameters are same as in Fig. 4.

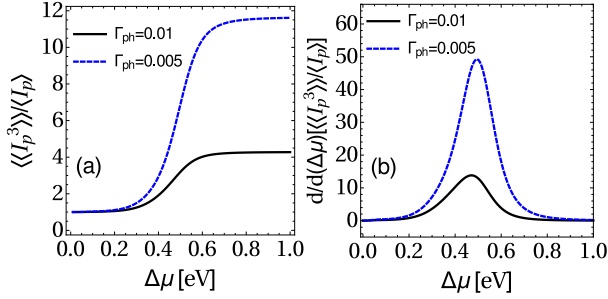


FIG. 7. (Color online) Third cumulant of charge transfer as obtained from QME and NEGF (overlapping). We used $\Gamma = 0.1$ eV, other parameters are same as in Fig. (4).

tively. We find that results obtained from QME calculation exactly match NEGF, even beyond the weak-coupling regime, for $\Gamma = 0.1$ eV.

B. Scaling relations at high bias

We derive here scaling relations for the mean phonon number and transport quantities, current and high order cumulants, in the limit of low electronic temperature and high bias. We further assume strong metal-molecule coupling and isolate the primary mode from the secondary phonon bath, $\Gamma_{\text{ph}} = 0$. In the wide band approximation, we can write down the spectral function as $J_\alpha(\omega) = 4g/\Gamma_\alpha$, $\alpha = L, R$. We now introduce the notation $\bar{g}^2 = 8g^2/\pi$, assume a zero electronic temperature and apply a large bias, $\Delta\mu = \mu_R - \mu_L \gg \epsilon_{d,a}, \omega_0$. The rates (12) reduce to

$$\begin{aligned} k_d &\approx k_d^{R \rightarrow L} \approx \frac{\bar{g}^2 \omega_0}{\Gamma_L \Gamma_R} \left(\frac{\Delta\mu}{\omega_0} + 1 \right), \\ k_u &\approx k_u^{R \rightarrow L} \approx \frac{\bar{g}^2 \omega_0}{\Gamma_L \Gamma_R} \left(\frac{\Delta\mu}{\omega_0} - 1 \right). \end{aligned} \quad (61)$$

In this limit, the average phonon number and the mean displacement for the oscillator are given as

$$\langle \hat{n} \rangle = \frac{1}{2} \left(\frac{\Delta\mu}{\omega_0} - 1 \right), \quad \langle \hat{X}^2 \rangle = \frac{\Delta\mu}{\omega_0}. \quad (62)$$

In analogy with the classical oscillator which satisfies equipartition (in terms of mean square displacement $= \frac{1}{2\omega_0} \langle X^2 \rangle$), we define the effective temperature, $T_{\text{eff}} = \Delta\mu/2$, which is solely determined by the voltage drop across the junction⁶⁸.

The cumulant generating function for charge current, can be simplified as well in this limit,

$$\mathcal{G}(\lambda_p) = \frac{\bar{g}^2 \omega_0}{\Gamma_L \Gamma_R} \left[1 - \sqrt{1 + \left(\frac{\Delta\mu^2}{\omega_0^2} - 1 \right) (1 - e^{2i\lambda_p})} \right]. \quad (63)$$

It yields the current and the noise as

$$\begin{aligned} \langle I_p \rangle &= \frac{\bar{g}^2 \omega_0}{\Gamma_L \Gamma_R} \left[\frac{\Delta\mu^2}{\omega_0^2} - 1 \right], \\ \langle S_p \rangle &= \frac{\bar{g}^2 \omega_0}{\Gamma_L \Gamma_R} \left[\frac{\Delta\mu^4}{\omega_0^4} - 1 \right]. \end{aligned} \quad (64)$$

The Fano factor now reduces to $F = 1 + (\Delta\mu/\omega_0)^2$, showing a $\Delta\mu^2$ scaling⁶⁹. It can be further demonstrated that leading-order nonlinear contributions of higher order cumulants obey the scaling relation

$$\frac{C_{n+1}}{C_n} \propto \left(\frac{\Delta\mu}{\omega_0} \right)^2, \quad (65)$$

with C_n as the n -th order cumulant. It is interesting to note the strong nonlinear dependence on bias in the present model. similarly to that obtained with the single-site Anderson-Holstein problem^{24,69,70}.

C. Charge rectification

The proposal for an organic molecular rectifier (diode), based on donor-acceptor molecules, had largely initiated the field of molecular electronics⁵⁸. It is thus interesting to test the operation of a charge diode in the present model system, to gather simple guidelines for optimizing this effect.

It is obvious that to act as a diode, the junction as sketched in Fig. 1 should possess a spatial asymmetry. This can be introduced e.g. by using distinct D and A units, to support asymmetric states, $\epsilon_d \neq \epsilon_a$. The metal-molecule hybridization energy should be made small though, so as not to conceal this asymmetry by level broadening. This situation parallels with design principles for standard tunneling diodes⁷¹⁻⁷³. We apply the voltage in a symmetric manner, and for simplicity, we keep the levels fixed, independent of bias. If $\epsilon_d < \epsilon_a$, the functionality of the system as a diode is expected to be optimized when $(\mu_R - \mu_L)/2 \sim \epsilon_a$; in the forward direction the two electronic levels are placed within the bias

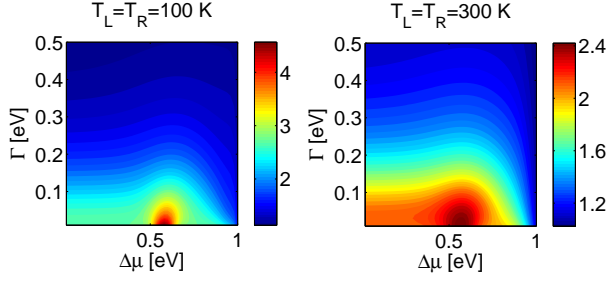


FIG. 8. (Color online) Rectification ratio in the donor-acceptor junction with $\epsilon_a = 0.2$, $\epsilon_d = 0$, $\omega_0 = 0.05$, $g = 0.01$, $\Gamma_{\text{ph}} = 0.005$ eV, and $T_{\text{ph}} = 300$ K. The temperature of the metal electrodes are (a) $T_L = T_R = 100$ K, and (b) $T_L = T_R = 300$ K.

window beneficial for conduction, while in the opposite bias ϵ_a is placed far away from μ_R . Fig. 8 presents a contour map of the rectification ratio, defined as

$$R \equiv \frac{\langle I_p \rangle_+}{|\langle I_p \rangle_-|}, \quad (66)$$

with $+$ ($-$) identifying the application of forward (reversed) bias, $\mu_R - \mu_L > 0$ ($\mu_L - \mu_R > 0$). Increasing the temperature of the metals washes away the diode behavior, as a electrons can cross the junction even when the Fermi function is placed in a region of low density of states. Similarly, reducing the frequency of the vibrational mode weakens the diode effect since even low-temperature electrons can excite the mode.

VI. CONCLUSION

We studied the non-equilibrium characteristics of vibrationally-assisted electronic conduction in a two-site junction, and demonstrated an equivalence between the QME and the NEGF approaches beyond the standard *weak* metal-molecule coupling regime. Examined non-equilibrium observables include the mean phonon number and the charge current and its higher fluctuations. Our study provided us with some important-general lessons: (i) Perturbation expansions. The master equation approach employed here was developed while taking into account all electron scattering processes with an exchange of a single quanta with the vibration. In the language of the NEGF, an RPA scheme had to be employed

for including all these processes, crucial for obtaining the correct steady state results.

(ii) Vibrational coherences. What role do vibrational coherences play in transport of electrons in our model, at weak electron-phonon coupling? While an NEGF-based derivation does not readily address this question, our QME method was based on rate equations for the populations of the vibrational states, decoupling the contribution of off-diagonal terms in the reduced density matrix. The agreement between these tools indicate that quantum coherences contribute to phonon occupation number and transport characteristics only in higher orders of the electron-vibration coupling.

(iii) Full counting statistics. NEGF theory provided us with a close analytical form for the CGF, [Eq. (40)]. One should note that the CGF was achieved here given the harmonic nature of the primary mode and its linear coupling—through its displacement—to the different environments. More complex models with e.g. anharmonic interactions, cannot be readily treated with the NEGF. In contrast, the QME approach as described here offers a straightforward program for simulating the current and its cumulants with general many-body molecular interactions.

Future studies will aim in reconciling QME and NEGF treatments in other models, e.g., when involving direct electron tunnelling between sites, and in generalizing the present results to include high order terms (strong) in electron-phonon interactions.

ACKNOWLEDGMENTS

This work was funded by an NSERC Discovery Grant, the Canada Research Chair program, and the CQIQC at the University of Toronto.

APPENDIX: COUNTING FIELD DEPENDENT BATH INDUCED RATES

The harmonic mode is coupled to metal electrodes and to a phonon environment. These baths induce transitions within the mode, and the rates are written in Sec. II. The current and its cumulants are reached by defining counting-fields dependent rates for processes driven by the electron baths. We identify these rates by the tilde symbol,

$$\begin{aligned} [\tilde{k}_d^{\text{el}}]^{L \rightarrow R} &= \int \frac{d\epsilon}{2\pi} f_L(\epsilon) (1 - f_R(\epsilon + \omega_0)) J_L(\epsilon) J_R(\epsilon + \omega_0) e^{-i(\lambda_p + (\epsilon + \omega_0)\lambda_e)}, \\ [\tilde{k}_d^{\text{el}}]^{R \rightarrow L} &= \int \frac{d\epsilon}{2\pi} f_R(\epsilon) (1 - f_L(\epsilon + \omega_0)) J_R(\epsilon) J_L(\epsilon + \omega_0) e^{i(\lambda_p + \epsilon\lambda_e)}, \\ \tilde{k}_u^{\text{el}} &= \tilde{k}_d^{\text{el}}[\omega_0 \rightarrow -\omega_0]. \end{aligned} \quad (\text{A1})$$

We further define the full electronic rates as

$$\tilde{k}_{u/d}^{\text{el}} = [\tilde{k}_{u/d}^{\text{el}}]^{L \rightarrow R} + [\tilde{k}_{u/d}^{\text{el}}]^{R \rightarrow L}, \quad (\text{A2})$$

and the total transition rates affecting the primary mode,

$$\tilde{k}_{u/d} = \tilde{k}_{\text{el}}^{u/d} + k_{u/d}^{\text{ph}}. \quad (\text{A3})$$

Note that processes induced by the phonon bath do not include here counting fields. We also define the difference between electronic rates as

$$\begin{aligned} (k_u^{\text{el}})' &\equiv \partial_{i\lambda_p} \tilde{k}_u^{\text{el}}|_{\lambda=0} = [k_u^{\text{el}}]^{R \rightarrow L} - [k_u^{\text{el}}]^{L \rightarrow R} \\ (k_d^{\text{el}})' &\equiv \partial_{i\lambda_p} \tilde{k}_d^{\text{el}}|_{\lambda=0} = [k_d^{\text{el}}]^{R \rightarrow L} - [k_d^{\text{el}}]^{L \rightarrow R}. \end{aligned} \quad (\text{A4})$$

These expressions come to play in the Born-Markov treatment of the characteristic function, Sec. IV B.

- ¹N. J. Tao, *Nature Nanotech.* **1**, 3 (2006).
- ²M. Galperin, M. A. Ratner, and A. Nitzan, *J. Phys.: Condens. Matter* **19**, 103201 (2007).
- ³S. Aradhya and L. Venkataraman, *Nature Nanotech.* **8**, 399 (2013).
- ⁴J. P. Bergfield and M. A. Ratner, *Physica Status Solidi (b)* **250**, 2249 (2013).
- ⁵C. M. Guëdon, H. Valkenier, T. Markussen, K. S. Thygesen, J. C. Hummelen, and S. van der Molen, *Nature Nanotech.* **7**, 305 (2012).
- ⁶H. Vazquez, R. Skouta, S. Schneebeli, M. Kamenetska, R. Breslow, L. Venkataraman, and M.S. Hybertsen, *Nature Nanotech.* **7**, 663 (2012).
- ⁷M. Elbing, R. Ochs, M. Koentopp, M. Fischer, C. von Hänisch, F. Weigend, F. Evers, H. B. Weber, and M. Mayor, *Proc. Natl. Acad. Sci.* **102**, 8815 (2005).
- ⁸B. Capozzi, J. Xia, O. Adak, E. Dell, Z. Liu, J. C. Taylor, J. B. Neaton, L. Campos, and L. Venkataraman, *Nature Nanotech.* **10**, 522 (2015).
- ⁹J. C. Cuevas and E. Scheer, *Molecular Electronics: An Introduction to Theory and Experiment*, World Scientific Series in Nanoscience and Nanotechnology, Singapore, (2010).
- ¹⁰J.-T. Lü, H. Zhou, J.-W. Jiang, and J.-S. Wang, *AIP Advances*, **5**, 053204 (2015).
- ¹¹J.-T. Lu, P. Hedegard, and M. Brandbyge, *Phys. Rev. Lett.* **107**, 046801 (2011).
- ¹²D. Segal, A. Nitzan, W. B. Davis, M. R. Wasielewski, and M. A. Ratner, *J. Phys. Chem. B* **104**, 3817 (2000).
- ¹³M. Galperin, A. Nitzan, and M. A. Ratner, *Phys. Rev. B* **74**, 075326 (2006).
- ¹⁴M. Galperin, A. Nitzan, and M. A. Ratner, *J. Chem. Phys.* **121**, 11965 (2004).
- ¹⁵T. L. Schmidt and A. Komnik, *Phys. Rev. B* **80**, 041307(R) (2009).
- ¹⁶O. Entin-Wohlman, Y. Imry, and A. Aharony, *Phys. Rev. B* **80**, 035417 (2009).
- ¹⁷R. Avriller and A. Levy Yeyati, *Phys. Rev. B* **80**, 041309(R) (2009).
- ¹⁸D. F. Urban, R. Avriller, and A. Levy Yeyati, *Phys. Rev. B* **82**, 121414(R) (2010).
- ¹⁹K. F. Albrecht, A. Martin-Rodero, R. C. Monreal, L. Mühlbacher, and A. Levy Yeyati, *Phys. Rev. B* **87**, 085127 (2013).
- ²⁰R. Egger and A. O. Gogolin, *Phys. Rev. B* **77**, 113405 (2008).
- ²¹R. Hützen, S. Weiss, M. Thorwart, and R. Egger, *Phys. Rev. B* **85**, 121408 (R) (2012).
- ²²C. Schinabeck, R. Härtle, H. B. Weber, and M. Thoss, *Phys. Rev. B* **90**, 075409 (2014).
- ²³L. Simine and D. Segal, *J. Chem. Phys.* **141**, 014704 (2014).
- ²⁴Y. Utsumi, O. Entin-Wohlman, A. Ueda, and A. Aharony, *Phys. Rev. B* **87**, 115407 (2013).
- ²⁵W. Dou, A. Nitzan, and J. E. Subotnik, *J. Chem. Phys.* **142**, 084110 (2015).
- ²⁶W. Dou, A. Nitzan, and J. E. Subotnik, *J. Chem. Phys.* **142**, 234106 (2015).
- ²⁷A. Zhugayevych and S. Tretiak, *Ann. Rev. Phys. Chem.* **66**, 305-330 (2015).
- ²⁸L. Simine and D. Segal, *Phys. Chem. Chem. Phys.* **14**, 13820 (2012).
- ²⁹L. Simine and D. Segal, *J. Chem. Phys.* **138**, 214111 (2013).
- ³⁰T. Markussen and K. S. Thygesen, *Phys. Rev. B* **89**, 085420 (2014).
- ³¹L. Simine, W. J. Chen, and D. Segal, *J. Phys. Chem. C* **119**, 12097 (2015).
- ³²B. K. Agarwalla, J. H. Jiang, and D. Segal, arXiv:1508.02475, *Phys. Rev. B* (2015).
- ³³B. K. Agarwalla, J. H. Jiang, and D. Segal, *Beilstein J. Nanotechnol.* **6**, 2129 (2015).
- ³⁴A. Erpenbeck, R. Härtle, and M. Thoss, *Phys. Rev. B* **91**, 195418 (2015).
- ³⁵E. L. Wolf, *Principles of Electron Tunneling Spectroscopy* (Oxford University Press, New York) 1985.
- ³⁶K. W. Hipps and U. Mazur, *J. Phys. Chem.* **97**, 7803 (1993).
- ³⁷M. A. Reed, *Materials Today* **11** 46 (2008).
- ³⁸S. Gustavsson, R. Leturcq, B. Simovic, R. Schleser, T. Ihn, P. Studerus, K. Ensslin, D. C. Driscoll, and A. C. Gossard, *Phys. Rev. Lett.* **96**, 076605 (2006).
- ³⁹T. Fujisawa, T. Hayashi, R. Tomita, and Y. Hirayama, *Science* **312**, 5780 (2006).
- ⁴⁰J.-S. Wang, B. K. Agarwalla, H. Li, and J. Thingna, *Front. Physics* **9**, 673 (2014).
- ⁴¹J. Rammer, *Quantum Field Theory of Non-Equilibrium States*, Cambridge: Cambridge University Press, (2007).
- ⁴²M. Di Ventra, *Electrical Transport in Nanoscale Systems*, Cambridge: Cambridge University Press, (2008).
- ⁴³H. Haug and A. P. Jauho, *Quantum Kinetics in Transport and Optics of Semiconductors*, Springer, (1996).
- ⁴⁴A. Dhar and D. Sen, *Phys. Rev. B* **73**, 085119 (2006).
- ⁴⁵J. Koch, F. von Oppen, Y. Oreg, and E. Sela, *Phys. Rev. B* **70**, 195107 (2004).
- ⁴⁶A. Mitra, I. Aleiner, and A. J. Millis, *Phys. Rev. B* **69**, 245302 (2004).
- ⁴⁷U. Harbola, M. Esposito, and S. Mukamel, *Phys. Rev. B* **74**, 235309 (2006).
- ⁴⁸D. Segal, *Phys. Rev. B* **73**, 205415 (2006).
- ⁴⁹S. Welack, M. Schreiber, and U. Kleinekathöfer, *J. Chem. Phys.* **124**, 044712 (2006).
- ⁵⁰M. Leijnse and M. R. Wegewijs, *Phys. Rev. B* **78**, 235424 (2008).
- ⁵¹J. Thingna, J.-S. Wang, and P. Hänggi, *Phys. Rev. E* **88**, 052127 (2013).
- ⁵²B. Popescu, H. Rahman, and U. Kleinekathöfer, *J. Chem. Phys.* **142**, 154103 (2015).
- ⁵³Y. Meir and N. S. Wingreen, *Phys. Rev. Lett.* **68**, 2512 (1992).
- ⁵⁴A. O. Gogolin and A. Komnik, *Phys. Rev. B*, **73**, 195301 (2006).
- ⁵⁵H. Li, B. K. Agarwalla, B. Li, and J.-S. Wang, *Eur. Phys. J. B* **86**, 500 (2013).
- ⁵⁶R. Volkovich, R. Härtle, M. Thoss, and U. Peskin, *Phys. Chem. Chem. Phys.* **13**, 14333 (2012).
- ⁵⁷M. Esposito, M. A. Ochoa, and M. Galperin, *Phys. Rev. B* **91**, 115417 (2015).
- ⁵⁸A. Aviram and M. A. Ratner, *Chem. Phys. Lett.* **29**, 277 (1974).
- ⁵⁹M. Esposito, U. Harbola, and S. Mukamel, *Rev. Mod. Phys.* **81**, 1665 (2009).
- ⁶⁰Y. Utsumi, D. S. Golubev, and G. Schön, *Phys. Rev. Lett.* **96**, 086803 (2006).
- ⁶¹A. Altland and B. D. Simons, *Condensed Matter Field Theory, 2nd edition*, Cambridge University Press, 2010.
- ⁶²H. P. Breuer and F. Petruccione, *The Theory of Open Quantum Systems* (Oxford University Press, Oxford, 2002).
- ⁶³H. Li, B. K. Agarwalla, and J.-S. Wang, *Phys. Rev. B* **86**, 165425 (2012).

- ⁶⁴M. Campisi, P. Hänggi, and P. Talkner, *Rev. Mod. Phys.* **83**, 771 (2011).
- ⁶⁵B. K. Agarwalla, B. Li, and J.-S. Wang, *Phys. Rev. E* **85**, 051142 (2012).
- ⁶⁶C. Flindt, T. Novotný, A. Braggio, M. Sasseti, and A. P. Jauho, *Phys. Rev. Lett.* **100**, 150601 (2008).
- ⁶⁷C. Flindt, T. Novotný, A. Braggio, and A. P. Jauho, *Phys. Rev. B* **82**, 155407 (2010).
- ⁶⁸D. Mozyrsky and I. Martin, *Phys. Rev. Lett.* **89**, 018301 (2002).
- ⁶⁹T. Novotný and W. Belzig, *Beilstein J. Nanotech.* **6**, 1853 (2015).
- ⁷⁰N. G. Van Kampen, *Stochastic processes in Physics and Chemistry*, 2nd ed; North Holland: Amsterdam, Netherlands, (1992).
- ⁷¹M. L. Perrin, E. Galan, R. Eelkema, F. Grozema, J. M. Thijssen, and H. S. J. van der Zant, *J. Phys. Chem. C* **119**, 5697 (2015).
- ⁷²C. Van Dyck and M. A. Ratner, *Nano Lett.* **15**, 1577 (2015).
- ⁷³M. Kilgour and D. Segal, *J. Phys. Chem. C* **119**, 25291 (2015).